Dynamic Features for Iris Recognition

Ronaldo Martins da Costa and Adilson Gonzaga, *Member, IEEE*

***Abstract*—The human eye is sensitive to visible light. Increasing illumination on the eye causes the pupil of the eye to contract, while decreasing illumination causes the pupil to dilate. Visible light causes specular reflections inside the iris ring. On the other hand, the human retina is less sensitive to near infra-red (NIR) radiation in the wavelength range from 800 nm to 1400 nm, but iris detail can still be imaged with NIR illumination. In order to measure the dynamic movement of the human pupil and iris while keeping the light-induced reflexes from affecting the quality of the digitalized image, this paper describes a device based on the consensual reflex. This biological phenomenon contracts and dilates the two pupils synchronously when illuminating one of the eyes by visible light. In this paper, we propose to capture images of the pupil of one eye using NIR illumination while illuminating the other eye using a visible-light pulse. This new approach extracts iris features called "dynamic features (DFs)." This innovative methodology proposes the extraction of information about the way the human eye reacts to light, and to use such information for biometric recognition purposes. The results demonstrate that these features are discriminating features, and, even using the Euclidean distance measure, an average accuracy of recognition of 99.1% was obtained. The proposed methodology has the potential to be "fraud-proof," because these DFs can only be extracted from living irises.**

***Index Terms*—Biometry, consensual reaction, consensual reflex, dynamic features, iris recognition.**

I. Introduction

RECENT INFORMATION technology advancements—as well as the enhancement in security requirements for accessing systems, security rooms, etc.—have driven the development of new research for the recognition of users by biometric techniques. Biometrics can be defined as the "science that studies the measurement of the living being." Biometric traits have been analyzed through the scientific literature, and the iris recognition has received special consideration due to the accuracy of recognition achieved by this methodology. Because of its own features, the iris provides means to individually identify each subject in a large population [1], [2]. It has been commonly known—since 1936—that the texture features of the human iris were potentially useful for discriminating individuals. In this year, Frank Burch, an eye specialist, suggested that these features could be employed for identifying subjects. The first theory of recognition using the iris was documented by James Daggarts in 1949 [3]. Since the theory by Daggarts, other iris recognition algorithms have been developed, such as the Wildes [5], Boles and Boashash [6] algorithms.

Compared to other biometric methods, iris recognition provides greater accuracy. For example, in 1993, Daugman [4] had already patented his method, which produces accuracy rates close to 99%.

Despite the high accuracy rates, most iris recognition methods are applied to static images, that is, the recognition is performed on a single image obtained under special near infrared (NIR) illumination conditions or under visible light. More recently, some studies using iris video images were reported [16], [17].

The first step in the biometric recognition process through the iris is pupil localization. Several algorithms use circle detection by the circular Hough transform [8] or by the integrodifferential operator [4], [3], [9], [10]. There are also hybrid methods with a combination of threshold, edge detectors, and the circular Hough transform [11]–[15]. Yet, as shown by John Daugman in 2007 [1], the pupil is not a perfect circle. As a result, a circle-supporting method to perform segmentation may omit important information and affect accuracy in a recognition process.

After the iris is segmented, different approaches are used in its codification. Daugman [4] proposed the codification of the iris pattern into a code named "IrisCode," with 256 bytes, by demodulation and use of a 2-D Gabor filter, representing the textures by phasors in the complex plane.

Other methods for the extraction of iris features are found in the literature, such as the cosine transform [19], the Markov model [15], the cumulative SUM [10], the convolution of a predetermined weight template upon a region of interest [12], a scale invariant feature transform-based algorithm [18], and direct linear discriminant analysis [19].

Daugman [4] implemented the recognition by a test with Boolean operations, such as XOR, applied to the 2048 bits. The XOR operator detects discordance between the pairs of bits. Then, it computes the Hamming distances (HD) as a dissimilarity measure between two irises. The shorter the HD is, the greater the similarity between the two irises becomes.

These iris recognition methodologies do not evaluate the known iris features together with, for example, the movements performed by the eye under illumination conditions. However, as the iris has a trabecular structure capable of altering its shape according to visual stimuli, it is assumed that these features can be altered differently in each subject, or that the evaluation of the pupil movement pattern can contribute to the recognition of a particular subject.

Manuscript received August 11, 2011; revised November 15, 2011 and January 17, 2012; accepted January 23, 2012. Date of publication February 29, 2012; date of current version July 13, 2012. This work was supported in part by FAPESP (State of São Paulo Research Foundation).

The authors are with the Electrical Engineering Department, University of São Paulo, São Carlos, 13566-590, Brazil (e-mail: ronaldomc12@gmail.com; agonzaga@sc.usp.br).

Color versions of one or more of the figures in this paper are available online at http://ieeexplore.ieee.org.

Digital Object Identifier 10.1109/TSMCB.2012.2186125

II. Objectives

To meet the increasing need for secure individual recognition, this paper suggests a new approach for recognition based on the human iris. This approach allows for both the evaluation of the texture features observed during pupil movements and the iris contraction and dilation rates due to the alteration of the illumination conditions. The purpose of this approach is to demonstrate that the dynamic features (DFs), that is, the features extracted during pupil contraction and dilation, can be employed efficiently in biometric recognition using the human iris.

III. Human Optic System Anatomy

The iris is a pigmented tissue, a trabecular meshwork, i.e., crossed filaments formed at the eighth month of pregnancy, between the cornea and the lens. Its surface is relatively flat, protected from external agents by the cornea, with a central orifice called the pupil. The iris has in its stroma a tissue meshwork located in its internal circle and dilator muscles that contract and dilate the pupil. The main function of the iris is to control, through the pupil, the amount of light entering the eye. The iris has a unique and complex structure for each individual. It is practically impossible for two irises to have the same texture. Therefore, iris biometrics is one of the most accurate methods of recognition. It is based on visible qualities, such as rings, grooves, spots, crowns, etc. The algorithms basically convert these visible features into a code, which will be the stored pattern for future comparison [20].

The human eye is sensitive to visible light; the pupil contracts and dilates depending on the intensity of visible light, and the iris and the sclera reflect light exceptionally well. Therefore, in capturing the image of the human iris under visible light, a question arises: how can the natural reflections on the globe of the eye, iris, and sclera surfaces be kept from affecting the quality of the digitalized image?

Several techniques are employed by professional photographers to avoid the reflected light beams from the eye by positioning the camera appropriately. However, in order to acquire iris images at a good resolution, allowing for the extraction of features required for biometric recognition, these photographic techniques cannot be used because the camera for iris recognition must be positioned in front of the iris and at a short distance, unlike photography.

Current systems for the acquisition of human iris images—for the purpose of recognition—have solved this problem by using images obtained by NIR light. In these systems, the eye is illuminated from the front with NIR light-emitting diodes (LEDs), and the image is captured and digitized with a camera sensitive to infra-red light, resulting in a gray image that minimizes light reflections on the iris, as can be seen on Fig. 1 [1], [21].

How can we capture images without visible light reflections while controlling the pupil contraction and dilation? Better yet, how can we capture iris images by NIR illumination while using visible light to contract and dilate the pupil without causing reflections on the iris, thus extracting the DFs, that is, features based on the pupil movements?

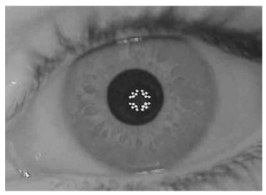

Fig. 1. NIR illumination eye image. A NIR illumination image usually presents good resolution. Nevertheless, the frequency of near infra-red light keeps the pupil from contracting and dilating.

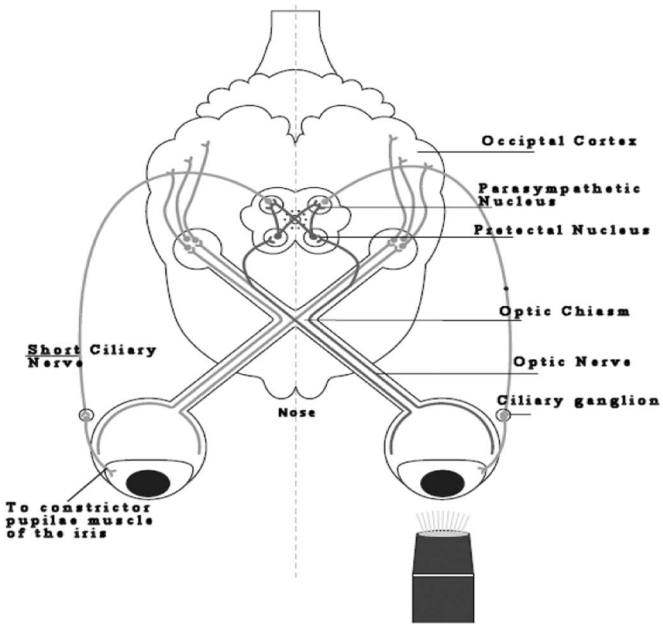

Fig. 2. Consensual reflex. Adapted from [27].

The answer lies in the anatomy of the human optic system. The eye captures, through the cones and rods, the light stimuli that is taken to the brain by the optic nerve for visual images to be processed [22]–[27].

If light illuminates one eye, the pupils of both eyes normally constrict. The constriction of the pupil upon which the light is illuminated is called the direct light reflex. The constriction of the opposite pupil, even though no light fell upon that eye, is called the consensual light reflex. The afferent nervous impulses travel from the retina through the optic nerve, the optic chiasma, and the optic tract. A small number of fibers leave the optic tract and the synapses on nerve cells in the pretectal nucleus. The impulses are passed by axons of the pretectal nerve cells to the parasympathetic nuclei of the oculomotor nerve on both sides.

The fiber synapse and the parasympathetic nerves travel through the oculomotor nerve to the ciliary ganglion in the orbit. Finally, postganglionic parasympathetic fibers pass through the short ciliary nerves to the eyeball and the constrictor pupillae muscle of the iris. Both pupils constrict in the consensual light reflex because the pretectal nucleus sends fibers to the parasympathetic nuclei on both sides of the midbrain as shown in Fig. 2 [22]–[27].

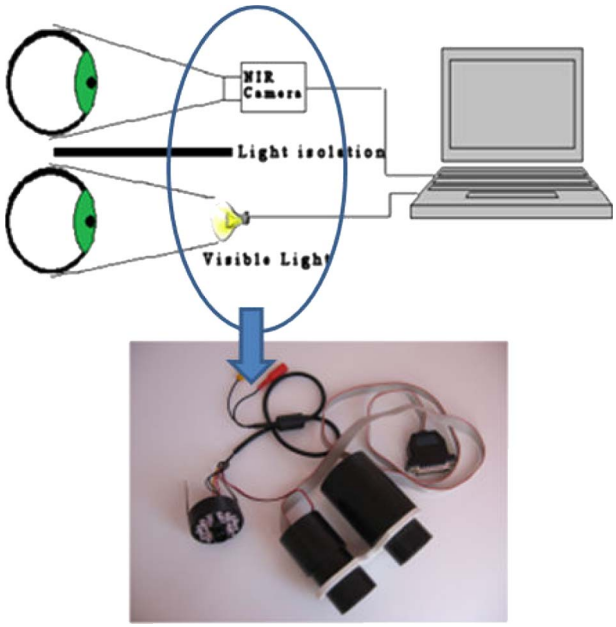

Fig. 3. Proposed device and prototype to capture iris images.

IV. Methodology

A. Material

Based on the "consensual reflex," a device was developed for the acquisition of iris images, as shown in Fig. 3. This device performs different and independent tasks on each eye. The right eye receives visible light stimuli (white light) at computer-controlled specific time intervals, while the left eye image is captured and digitized into a video sequence under NIR illumination. The two sides of the device related to the left and right eyes are isolated from each other.

The video sequence obtained under NIR illumination is synchronized with the "visible light" pulses (a white light LED was employed) applied to the other eye. Thus, it is possible to extract the features of the frames during pupil contraction or dilation without the interference of light reflections from the iris, pupil, and sclera. Their movements are induced by the light stimulus applied to the other eye and, due to the consensual reflex, repeated by the eye whose image is being digitized without interference from visible light reflections. A prototype was built so that the video sequences could be acquired. The prototype performs different and independent tasks on each eye. While the right eye is receiving computer-controlled visible light stimuli, it is basically impossible for the subject under study to know when the time intervals of illumination will take place. Therefore, there is almost no chance of fraud. The system depends on a living iris to respond to the previously programmed light stimuli.

The prototype has a camera sensitive to NIR radiation, whose characteristics are: NTSC, 510 × 492 pixels of resolution, NIR sensitive at 850 nm. The camera was positioned at a fixed focal distance of 5.2 cm from the eye.

A 20-LED set operating in the range of NIR light, installed around the lens and parallel to its optic axis, provides illumination of the front of the eye whose image is being digitized.

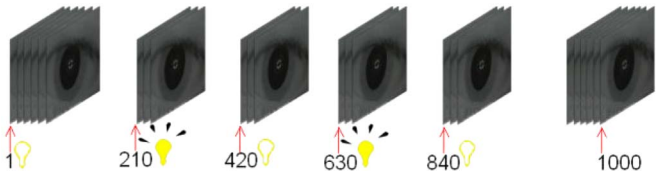

Fig. 4. Light stimuli intervals during video sequence acquisition.

TABLE I
Visible Light (LED) Control

Frames	*Visible light (LED)*
1 to 209	Off
210 to 419	On
420 to 629	Off
630 to 839	On
840 to 1000	Off

In order to digitize the video sequences, we used a frame-capture board with a USB 2.0 interface by PixelView running at 30 frames/s. The reflex caused by the infra-red LED takes place solely on the pupil but not on the iris. Reflecting the NIR illumination is a biological feature of the retina and does not compromise the image quality of the iris to be analyzed by segmentation.

B. Video Capture

During the capture of each image sequence, we applied visible light pulses to the eye not being digitalized using the white LED, whereas the camera digitizes the image sequence of the other eye that is illuminated in the NIR band. Fig. 4 shows the time intervals determined by our proposed methodology for the measurement of the DFs of the iris. These intervals were defined empirically and can be altered by the control software. Table I shows the visible light LED controlled operation illuminating the right eye in the pre-established time intervals.

We captured videos from 111 people in a maximum period of 120 days between the first and last video—five videos of each—totaling 555 videos, with 1000 frames per video sequence.

C. Preprocessing and Iris Segmentation

In order to segment the iris, we have to exclude the regions that will interfere with the recognition, such as the eyelashes and the eyelids. Due to eye movements, it is necessary to delete those frames that cannot be used for the recognition method and select only the adequate ones. The algorithm excludes the inadequate frames and employs the remaining ones. In the proposed method, capturing a new video requires a longer capture time for the subject, possibly causing some discomfort to the subject.

The problems which may lead a frame to be excluded during preprocessing can be seen in Fig. 5, and are "frowned" eyes (Fig. 5(a)), closed eyes (Fig. 5(b)), "off-angle" eyes (Fig. 5(c)), and an unfocused image (Fig. 5(d)).

1) Discarding Unfocused Images and Improper Frames: Some frames can be unfocused or smudgy, which may affect the extracted features.

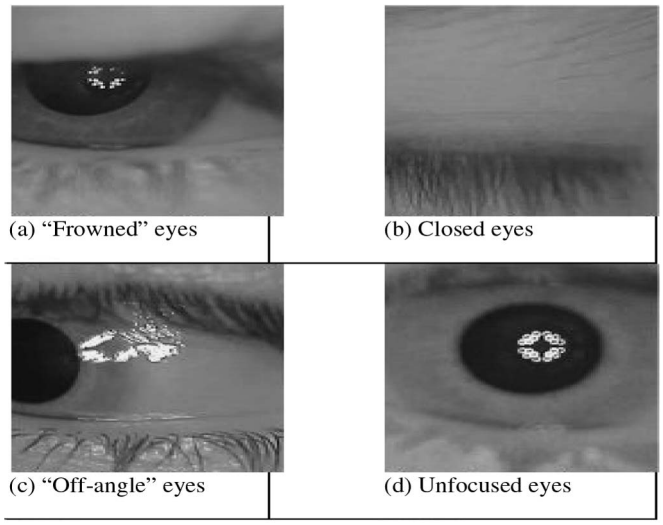

Fig. 5. Improper frames. (a) "Frowned" eyes. (b) Closed eyes. (c) "Off-angle" eyes. (d) Unfocused image.

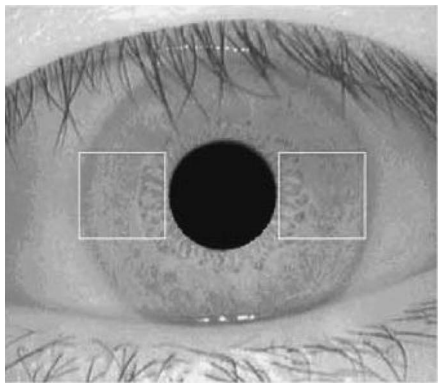

Fig. 6. Two image portions analyzed, in the iris area, with a dimension of 22×22 pixels.

In order to diminish the influence of these errors, two image portions are analyzed in the iris area to determine if the image is adequate for analysis. Each image has a dimension of 22×22 pixels, as shown at Fig. 6. We calculated the 2-D Fourier spectrum of each portion, resulting in two 22×22 bidimensional matrices, and determined a quality indicator (Q) shown in (1).

Compared to images of low quality, a clear and properly focused iris image has a relatively uniform frequency distribution.

$$Q=\left[(F_1+F_2+F_3);\frac{F_2}{(F_1+F_3)}\right]$$
$$F_i=\int\limits_{\Omega=\left\{(u,v)|f_1^i<\sqrt{u^2+v^2}\le f_2^i\right\}}\int |F(u,v)dudv|\ i=1,2,3 \quad (1)$$

where $F(u,v)$ is the 2-D Fourier spectrum of an iris region, F_1, F_2, and F_3 are the power of the low-, middle-, and high-frequency components, respectively, f_1^i and f_2^i are the radial frequency pair and are bound by the range of the corresponding frequency components.

The quality descriptor, Q, consists of two discriminating frequency features. The first feature is the total spectral power of an iris region, which can effectively discriminate clear iris images from severely damaged iris images. The second feature is the ratio of the middle-frequency power to the frequency power of the other frequency components. It should be larger for the clear image than for the defocused and motion blurred image because the former has much more middle-frequency information. We used the Euclidean distance to distinguish whether the corresponding iris image is clear or not.

Fig. 7. Example of a segmented iris.

Ideal values for Q are values less than $Q = [6.8; 0.425]$. Larger Q values mean that the frame must be discarded as an "unfocused image." Proper frames are those in which the pupil is located near the center.

2) Iris Segmentation: For pupil detection and iris segmentation, our approach is very simple and fast, because we need information, frame by frame, from both the pupil diameter variation and the iris texture, at video rates. We used the Sobel edge detector and the Hough transform for circles [8].

Moreover, we cut the segmented iris on the top and bottom, taking into account a horizontal tangent to the pupil border, thereby generating two sectors (Sector A and Sector B), as shown in Fig. 7. These areas are excluded because they contain information that can compromise the image evaluation, such as eyelashes, eyelid, and sclera. The change in texture due to iris contraction/dilation process will be measured, frame by frame, over these two sectors.

D. Dynamic Features

A challenge in the proposed approach is related to the extraction of the discriminating DFs. The primary movement that occurs in the globe of the eye submitted to a light stimulus is pupil contraction and dilation [22]–[27]. In order to define which features must be evaluated to verify its discrimination potential, we have defined as "DFs" those related to the pupil movement during the light stimuli, that is:

a) Features of pupil contraction and dilation.
b) Iris texture properties during pupil contraction and dilation.

Twelve different features were defined and noted in Table II. We analyzed these features one by one to verify the discrimination potential among different segmented irises. The first four features are directly related to pupil contraction and dilation, and the other ones are related to the texture properties in the iris area that are measured in intervals with and without illumination.

With our prototype, we captured a video database. Each video has 1000 frames digitized on predefined intervals of light stimuli.

TABLE II
PROPOSED DYNAMIC FEATURES

N	Feature
1)	Pupil circularity
2)	Pupil diameter
3)	Pupil contraction/dilation time
4)	Pupil contraction/dilation rate
5)	Gray level average of the segmented iris
6)	Gray level standard deviation of the segmented iris
7)	Gray level variation coefficient of the segmented iris
8)	Correlation (0º, 45º, 90º and 135º)
9)	Angular Second Moment (ASM) (0º, 45º, 90º and 135º)
10)	Entropy (0º, 45º, 90º and 135º)
11)	Contrast (0º, 45º, 90º and 135º)
12)	Inverse Difference Moment (IDM) (0º, 45º, 90º and 135º)

We established five periods for data analysis. The first period is composed of all the adequate frames of the video, and the other ones are defined so that the illumination transition period could be obtained, capturing the alterations taking place in this transition.

The periods comprise the following frames:

- First period—all the 1000 frames
- Second transition period—from frame 210 to 220
- Third transition period—from frame 420 to 430
- Fourth transition period—from frame 630 to 640
- Fifth transition period—from frame 840 to 850

E. Features of Pupil Contraction and Dilation

1) Circularity: The pupil, in most cases, is not a perfect circle. Because the pupil is formed by muscles (trabeculae) [22]–[27], the contraction and dilation can disfigure this pseudocircle even more. The pupil is better approximated by an ellipse. Both contraction/dilation and circularity measured over time are features that differ from person to person. In order to verify the discrimination potential of iris circularity among the subjects, an analysis on this property was performed for five people.

The pupil circularity is given by (2) (see Fig. 8).

$$C = A/a \tag{2}$$

where

C is the circularity,
A is the pupil's major axis, and
a is the pupil's minor axis.

When we apply a visible light pulse onto the right eye, both the right and left pupil contract, and when the light is turned off, both pupils dilate. The pupil circularity is altered during the contraction and dilation times and is measured frame by frame during the referred transition periods (from the second to the fifth).

By using circularity, we extracted five features: the overall mean circularity of all frames and the four mean values from the second to the fifth transition periods.

2) Diameter: The pupil diameter is another dynamic characteristic contributing to recognition, and it is determined by the major axis measurement.

The pupil diameter provides DFs to the recognition task, such as the contraction and dilation times and the pupil contraction and dilation rates as a function of the applied stimuli.

We extracted 13 features using the diameter measurement:

a) The overall diameter mean value for all the frames—one feature;
b) The diameter mean values from the second to the fifth transition period—four features;
c) The pupil contraction rate in the second and fourth transition periods—two features;
d) The pupil dilation rate in the third and fifth transition periods—two features;
e) The pupil contraction time in the second and fourth transition periods—two features;
f) The pupil dilation time in the third and fifth transition periods—two features.

3) Pupil Contraction and Dilation Rates: Fig. 9 presents a graph of the pupil diameter variation for a subject. As highlighted, the pupil contracts more in the first light pulse, between frames 210 and 220 (second transition period), than between frames 630 and 640 (fourth transition period), when the second light pulse takes place. The mean values for this variation are used as a feature for each subject.

The pupil contraction or dilation rates are calculated from the diameter variation, within the specified transition period, between a minimum and a maximum value. We extracted four DFs, measured at each interval transition. In the transition from interval 1 to 2 and from interval 3 to 4, the illumination is on, and the pupil is contracted, leading to the two contraction rates calculated by (4). In the transition from interval 2 to 3 and from interval 4 to 5, the illumination is turned off, causing the pupil to dilate, leading to the two dilation rates calculated by (5), where

Δc is the contraction rate, that is, how much the diameter is reduced over time, indicated by D^-
Δd is the dilation rate, that is, how much the diameter is increased over time, indicated by D^+

$$\Delta c = \frac{\partial D^-}{\partial t} \tag{3}$$

$$\Delta c = \frac{\partial D^+}{\partial t}. \tag{4}$$

4) Pupil Contraction and Dilation Time: After a certain period of time from the initiation of the illumination pulse, the pupil diameter achieves its maximum contraction, and, after the illumination is turned off, the diameter achieves the maximum dilation and then is stable. The area highlighted in Fig. 9 shows the diameter alteration in the transition area (light pulse applied at frame 210), the minimum diameter achieved (maximum contraction) and finally the gradual return to the mean stabilized value. We measured the contraction and dilation time in "number of frames" because the camera acquisition rate is constant (30 frames per second (FPS)).

We established the number of 50 frames as a maximum limit for the evaluation, thus avoiding errors generated during the

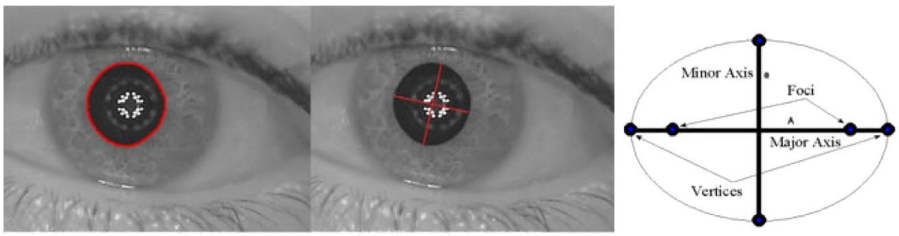

Fig. 8. Pupil circularity

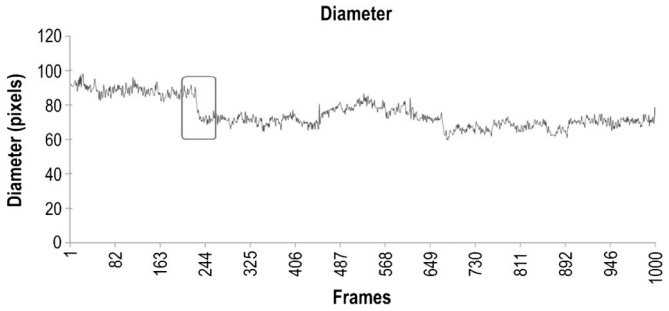

Fig. 9. Pupil diameter variation for a subject.

acquisition stage due to the person's reaction to white light. The highest/lowest value within this range is assumed to be the maximum contraction/dilation. We extracted four more features using this measure, taken during the interval transition. During the transition from interval 1 to 2 and from interval 3 to 4, the illumination is on, and the pupil is contracted, leading to the two contraction times. In the transition from interval 2 to 3 and from interval 4 to 5, the illumination is turned off and the pupil dilates, leading to the two dilation times.

F. Iris Texture Properties During Pupil Contraction and Dilation

To extract the iris texture features, we used second-order statistics [29]. Iris texture has been commonly utilized in static image recognition [4]. Many structures found in the texture of iris images provide important information in their statistical classification. The first-order statistical measures are limited as texture descriptors because there is no consideration regarding the relative position of the gray levels in a certain image. Second-order statistics solve this problem by considering the relative position of the pixels.

The second-order statistical measures are obtained from the second-order probability distribution [30] or from co-occurrence matrices. When an image is analyzed, a dipole r is positioned on the image of a specific size and direction. When two pixels with intensity $x0$ coincide with the dipole ends, an occurrence counter for pairs of pixels with intensity $x0$ is incremented. In order to calculate the occurrence probability for the pixels $x0$ in the image, the number of occurrences is divided by the maximum number of possible occurrences, under the conditions imposed by the size and direction of the dipole r.

Therefore, if the gray level distribution in two images is different, the probability for the dipole $p(r)$ of touching two points in each image is different.

1) Gray Level Mean Values: The gray levels are not under the influence of illumination because the image is acquired using NIR illumination that does not cause pupil reactions.

We extracted ten features using the gray level mean values; five for iris sector A and five for iris sector B (see Fig. 7).

2) Gray Level Standard Deviation: The standard deviation is the iris gray level deviation around the mean value in the established sector and periods.

By using the standard deviation, we extracted ten features; five for iris sector A and five for iris sector B (see Fig. 7).

3) Gray Level Variation Coefficient: The variation coefficient is given by (5) and represents the iris gray level variation coefficients for the two sectors and in the five periods considered

$$VC = \frac{S}{\overline{x}} \tag{5}$$

where

S is the standard deviation and
$\overline{x}$ is the gray level mean value.

We extracted ten features using the gray level variation coefficient; five for iris sector A and five for iris sector B.

4) Angular Second Moment: The Angular Second Moment (ASM) is a measure that evaluates the texture uniformity, which is the repetition of pairs of gray levels. When the area of interest shows uniform texture (values of gray levels close to each other), the energy value tends toward 1. In case the area is not uniform, the energy value tends toward 0 (zero). The ASM is given by

$$ASM = \sum_{i=1}^{n}\sum_{j=1}^{n}\left(\frac{p(i,j,d,\theta)}{i\cdot j}\right)^2 \tag{6}$$

where (i,j) are the lines and columns of the co-occurrence matrices, $p(i,j,d,\theta)$ is the value for the line cell i, column j, at distance d, and angle θ.

We extracted 40 features using the ASM measure; 20 features for iris sector A and 20 features for iris sector B.

5) Correlation: Correlation measures the linear dependence among the gray levels of pairs of pixels. Values close to 1 imply a strong relationship between the gray levels of the pixels. The "Correlation" measure is not correlated to the ASM, that is, high correlation values can be found in low or high energy ASM values for the same area of interest. Correlation is given by

$$COR = \frac{\sum_{i=1}^{n}\sum_{j=1}^{n}\frac{i\cdot j\cdot p(i,j,d,\theta)}{i\cdot j} - \mu i\cdot\mu j}{\sigma i\cdot\sigma j} \tag{7}$$

where $p(i, j, d, \theta)$ is the value for the line cell i, column j, at distance d, and angle θ, considering the co-occurrence matrices

$$\mu i = \sum_{i=1}^{n}\sum_{j=1}^{n} \frac{i \cdot p(i,j,d,\theta)}{i \cdot j}$$

$$\mu j = \sum_{i=1}^{n}\sum_{j=1}^{n} \frac{j \cdot p(i,j,d,\theta)}{i \cdot j}$$

$$\sigma i = \sqrt{\sum_{i=1}^{n}\sum_{j=1}^{n} \frac{i^2 \cdot p(i,j,d,\theta)}{i \cdot j} - \mu i^2}$$

$$\sigma j = \sqrt{\sum_{i=1}^{n}\sum_{j=1}^{n} \frac{j^2 \cdot p(i,j,d,\theta)}{i \cdot j} - \mu j^2}.$$

We extracted 40 features by determining correlation values; 20 for each iris sector.

6) Entropy: When the image does not possess uniform texture, the entropy values tend to be very low. The entropy reaches its maximum value when the pixels in the area of interest show gray levels with random values. The entropy shows a negative linear correlation with the ASM, and it is not correlated to the correlation measure. Entropy is given by

$$ENT = \sum_{i=1}^{n}\sum_{j=1}^{n} \frac{p(i,j,d,\theta)}{i \cdot j} \cdot \log\left(\frac{i \cdot j}{p(i,j,d,\theta)}\right) \quad (8)$$

where $p(i, j, d, \theta)$ is the value for the line cell i, column j, at distance d, and angle θ, considering the co-occurrence matrices.

We extracted 40 features by using the entropy; 20 for each iris sector.

7) Contrast: Contrast measures the presence of a sudden transition of gray levels. The contrast is given by (9).

$$CON = \sum_{i=1}^{n}\sum_{i=1}^{n} \frac{(i-j)^2 \cdot p(i,j,d,\theta)}{i \cdot j} \quad (9)$$

where $p(i, j, d, \theta)$ is the value for the line cell i, column j, at distance d, and angle θ, considering the co-occurrence matrices.

We extracted 40 features by using Contrast; 20 for each iris sector.

8) Inverse Difference Moment: When the concentration of values in the co-occurrence matrix diagonal reaches the maximum value, the IDM reaches the maximum value. The (10) provides the inverse difference moment (IDM) value

$$IDM = \sum_{i=1}^{n}\sum_{i=1}^{n} \frac{1}{1+(i-j)^2} \cdot p(i,j,d,\theta) \quad (10)$$

where $p(i, j, d, \theta)$ is the value for the line cell i, column j, at distance d, and angle θ, considering the co-occurrence matrices.

We extracted 40 features by determining the mean of the IDM; 20 for each iris sector.

Because the values of the feature vector are different, this results in having more weight for one measure relative to the other; each of these measures is normalized to its maximum according to

$$z_i = \frac{x_i}{x_m} \quad (11)$$

where,

z_i is the normalized feature,
x_i is the extracted feature,
x_m is the maximum value of the extracted feature

By taking into account all the video sequence periods, we initially proposed a feature vector with 248 elements, ordered according to Table III.

TABLE III
FEATURE VECTOR FOR A VIDEO SEQUENCE

Feature Number	Feature	Number of Elements per Feature
1	Pupil circularity	5
2	Pupil diameter	5
3	Pupil contraction / dilation time	4
4	Pupil contraction / dilation rate	4
5	Gray level average of the segmented iris	10
6	Gray level standard deviation of the segmented iris	10
7	Gray level variation coefficient of the segmented iris	10
8	Correlation	40
9	Angular Second Moment (ASM)	40
10	Entropy	40
11	Contrast	40
12	Inverse Difference Moment	40
	Total of Vector Elements:	248

V. FEATURE SELECTION

In the analysis performed with five subjects, the iris features were discriminating when assessed alone. However, when working with a large amount of information, studies indicate the need to perform data mining so that the impact on the use of different measures together can be precisely evaluated, as proposed in the method.

Data mining is employed in the selection of features with a greater discrimination potential, thus optimizing the process with a reduction in the features applied. However, more than just simply obtaining this information reduction, this process allows for the generation of ways to predict future standard occurrences.

In order to accomplish the data mining task, we used the Weka software [31].

From the 248 DFs extracted, 17 were indicated by the data mining processing as the most discriminating ones, as seen in Table IV. For selection of the attributes, we applied the wrapper algorithm that performs internal cross-validation on the training data in order to determine the merit of a given subset of attributes.

TABLE IV
DYNAMIC FEATURES SELECTED BY DATA MINING

Feature	*Description*
Dilation	Pupil dilation time from frames 420 to 430
DilationRate1	Pupil contraction / dilation rate from frames 630 to 640
DilationRate2	Pupil contraction / dilation rate from frames 840 to 850
Average1	Gray level average of the B sector of the segmented iris for all the 1,000 frames of the video
Average2	Gray level average of the B sector of the segmented iris from frames 420 to 430
Average3	Gray level average of the B sector of the segmented iris from frames 630 to 640
Correlation1	Correlation of the A sector in the 90º angle of the co-occurrence matrix for all the 1,000 frames of the video
Correlation2	Correlation of the B sector in the 0º angle of the co-occurrence matrix from frames 210 to 220
Correlation3	Correlation of the B sector in the 90º angle of the co-occurrence matrix from frames 630 to 640
Correlation4	Correlation of the B sector in the 135º angle of the co-occurrence matrix from frames 840 to 850
ASM1	ASM of the A sector in the 0º angle of the co-occurrence matrix from frames 630 to 640
ASM2	ASM of the A sector in the 90º angle of the co-occurrence matrix from frames 630 to 640
ASM3	ASM of the B sector in the 135º angle of the co-occurrence matrix from frames 840 to 850
Entropy	Entropy of the A sector in the 135º angle of the co-occurrence matrix for all the 1,000 frames of the video
Contrast1	Contrast of the A sector in the 45º angle of the co-occurrence matrix from frames 840 to 850
Contrast2	Contrast of the B sector in the 45º angle of the co-occurrence matrix from frames 210 to 220
Contrast3	Contrast of the B sector in the 45º angle of the co-occurrence matrix from frames 630 to 640

VI. RESULTS

The results shown utilize, a total of 555 videos (111 subjects with five videos for each subject), each of which having a sequence of 1000 frames. In order to validate the results, we applied a cross-validation k-fold test with $k = 5$. It is expected that among the iris images of the same person, the distance between the feature vectors will be short, whereas among the iris images of different people, the distance be greater.

We used the Euclidean distance for the method validation, and Fig. 10 shows the Recall x Precision curve with the feature vector full (248 features) and with the vector containing only the selected features (17 features) by the data mining software. Precision (P) is the fraction of retrieved iris images that are relevant to the search, and Recall (R) is the fraction of the iris images that are relevant to the query that are successfully retrieved, and they are defined as:

$$P = \frac{tp}{tp + fp} \qquad R = \frac{tp}{tp + fn}$$

where, t_p is the number of true positives, f_p is the number of false positives, and f_n is the number of false negatives.

We also tested the algorithm performance by the cumulative match score (CMS) [7] curve, both before the feature selection and after the feature selection. These curves can be seen in Fig. 11.

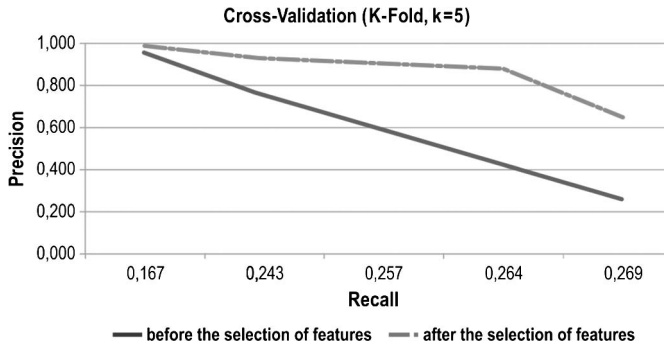

Fig. 10. Recall x Precision curve before and after feature selection.

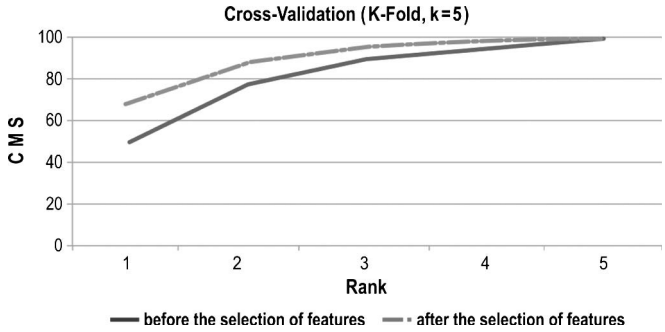

Fig. 11. CMS curve before and after feature selection.

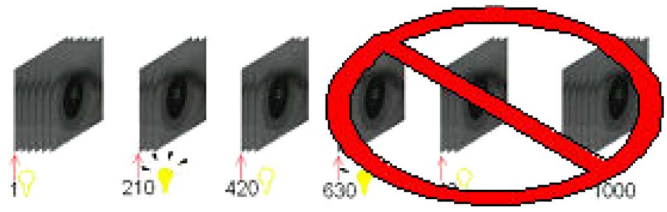

Fig. 12. Reduction of the evaluated intervals.

The results obtained demonstrated an outstanding discrimination potential for the dynamic characteristics proposed in this paper. However, for the prototype developed, operating at 30 FPS, capturing a video with 1000 frames means an exposure time of 33.33 s for each subject. This period of time can be uncomfortable for the subjects, leading to poor video quality, in addition to being practically unfeasible for the recognition of people.

By considering the first accommodation interval (frames 1 to 209) as equivalent to the intervals 3 and 5 (with the light stimulus on) and the interval 2 equivalent to the interval 4 (without the light stimulus), we implemented an alternative method in order to reduce the exposure time. We changed our acquisition time by using only the intervals 1 and 2 for evaluation, as shown in Fig. 12. The new feature vector has the illumination transition information, which occurs from frames 210 to 220 and from frames 420 to 430.

With this reduced number of time intervals, the new exposure time is now 14 s, a significant reduction compared with the exposure time for the previous 1000-frame model. The number of elements in the feature vector is also reduced because the

TABLE V
NEW FEATURE VECTOR OF A VIDEO SEQUENCE

Feature number	Feature	Number of Elements per Feature
1	Pupil Circularity	2
2	Pupil Diameter	2
3	Pupil contraction / dilation time	2
4	Pupil contraction / dilation rate	2
5	Gray level average of the segmented iris	4
6	Gray level standard deviation of the segmented iris	4
7	Gray level variation coefficient of the segmented iris	4
8	Correlation	16
9	Angular Second Moment	16
10	Entropy	16
11	Contrast	16
12	Inverse Difference Moment	16
	Total of Elements in the Vector:	**100**

TABLE VI
NEW DYNAMIC FEATURES SELECTED BY DATA MINING

Feature	Description
Dilation	Pupil dilation time from frames 420 to 430
Average2	Gray level average of the B sector of the segmented iris from frames 420 to 430
Correlation2	Correlation of the B sector in the 0º angle of the co-occurrence matrix from frames 210 to 220
Contrast2	Contrast of the B sector in the 45º angle of the co-occurrence matrix from frames 210 to 220
Contrast4	Contrast of the B sector in the 45º angle of the co-occurrence matrix from frames 420 to 430

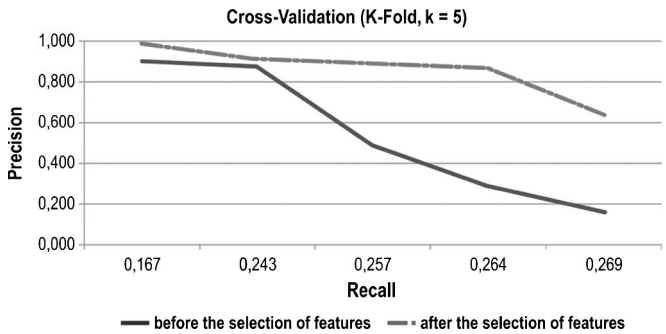

Fig. 13. Recall x Precision curve taking into account two intervals.

analysis is performed only in the two initial video periods. Table V shows the new reduced feature vector before data mining.

As was done with the previous 1000-frame model, we performed tests using only two time intervals with data mining, resulting in a reduction from 100 to only 5 discriminating features, as shown in Table VI. Fig. 13 shows the Recall x Precision curve by using Euclidean distance metrics using only two video intervals, both before and after the selection of features, by data mining.

The method performance using two video intervals was also evaluated by the CMS curve (Fig. 14), both before and after the feature selection, by data mining.

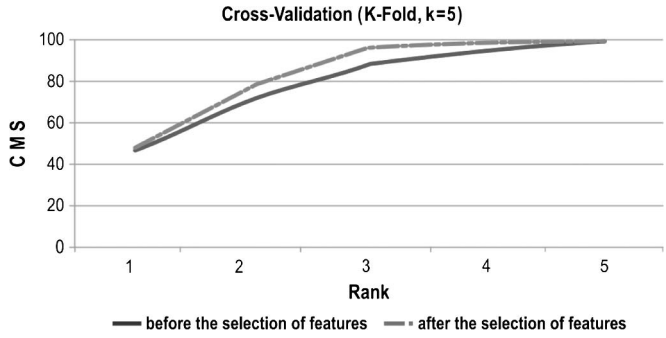

Fig. 14. CMS curve taking into account two intervals.

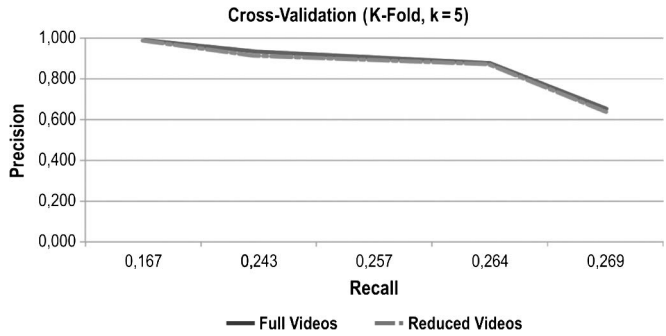

Fig. 15. Recall x Precision curve for five (full videos) and two (reduced videos) illumination intervals after feature selection.

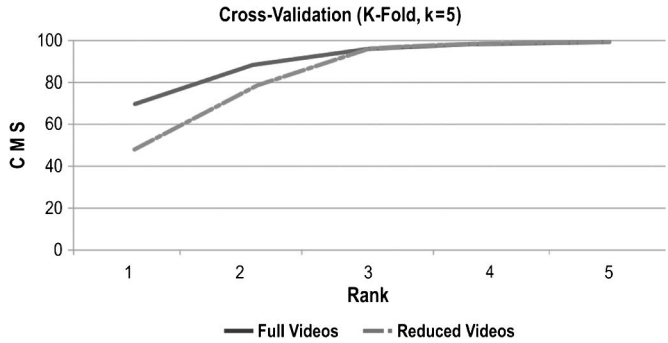

Fig. 16. CMS curve for five (full videos) and two (reduced videos) intervals after feature selection.

Fig. 15 shows the comparison of the results considering the two analyses performed, that is, on the complete videos, with 1000 frames and on the reduced videos, with 420 frames. In both analyses, the best results were obtained after feature selection. Fig. 16 shows the best results by the CMS curve.

For comparison, we took the best frames (ten frames with the lowest values for Q) of each video and applied Daugman's method [1].

Table VII shows the average accuracy, the equal error rate and the confidence interval of 95% for Daugman's method compared to our approach and Fig. 17 shows the detection error tradeoff curve (DET). The results demonstrate that these features are discriminating features, and, even using the Euclidean distance measure, an average accuracy of recognition of 99.1% was obtained.

TABLE VII
AVERAGE ACCURACY COMPARED

Method	Average Accuracy (AA) (%)	Confidence Interval (95%)	ERR (%)
Daugman [1]	99.5	99,426≤AA≤99,574	0.047
Dynamic Features	99.1	98,809≤AA≤99,391	0.049

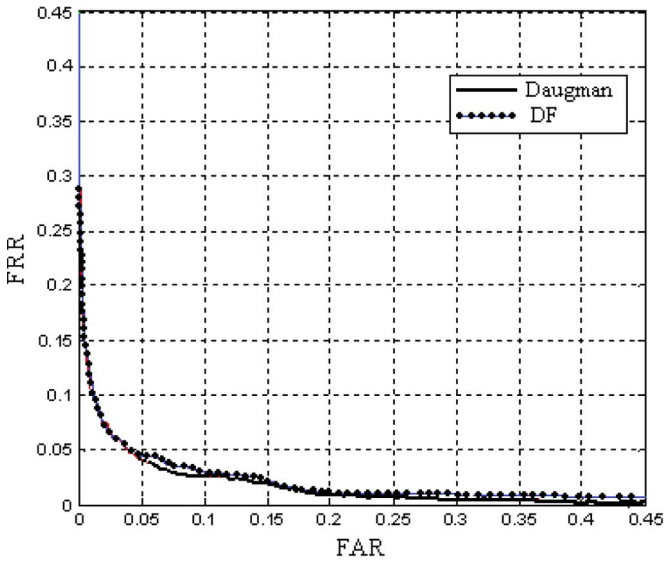

Fig. 17. DET curve for the dynamic features (DF) and Daugman's method [1]. FAR = false accept rate. FRR = false reject rate.

VII. CONCLUSION

This innovative methodology proposes the extraction of information about the way the human eye reacts to light, and to use such information for biometric recognition purposes. The results presented here demonstrated a minimum accuracy difference between the analyses performed with the full video versus the analysis with the reduced video, particularly in the evaluation by the Recall x Precision.

What is the shortest video time needed to recognize a subject? The results demonstrate that only two video intervals with a change in the illumination conditions are sufficient. And what is the ideal duration for each interval? It is likely that the intervals are different for different subjects.

One of the DFs that can be a limit is the pupil contraction/dilation time after the change in illumination conditions. In the evaluation of the 111 subjects, the meantime to stabilize the pupil contraction/dilation is around 50 frames, that is, from 2 to 3 s. This stabilization time indicates that a video with a duration of over 5 s (100 frames) and with a change in the illumination conditions during this time interval is necessary to accomplish the recognition task.

Recognition methods that utilize static iris images provide a high accuracy rate. We did a fair accuracy comparison between a static method (Daugman) and our method using the ten best frames from each video. Considering our acquired images, the DFs presented an excellent performance. Moreover, a simple similarity measure, based on the Euclidean distance, was employed in this paper, but is not employed by the static methods.

The results demonstrate that the iris DFs, proposed by our methodology, are discriminating, and may be employed for personal identification. In addition, the possibility to extract DFs from living irises could increase the resistance of our approach to fraud attempts in personal identification.

We argue that if a specific anticounterfeit technique followed by a classical recognition technique is used, the extracted iris features would still be static characteristics. We think that it could be a reasonable solution, and we hope to compare our approach with them, as soon these methods could be implemented. However, our methodology captures new information about the human's eye reaction under visible-light radiation. This approach has never been used in the published literature, until now, and the proposed DFs must be improved for better precision.

The tests demonstrate that, in addition to recognizing a person, the proposed method also authorizes the validation of certain attributes which the traditional methods for static images are not able to do. For example, the proposed method can check if the input image being analyzed is actually from a "living iris" or not by determining if the subject to be validated responds to the illumination stimuli applied, or if the subject is using artificial irises in an attempt to cheat the recognition method. In addition to personal recognition, the methodology proposed also allows for the evaluation of the iris behavior at different moments under different illumination stimuli.

The device built, conceived for this methodology, presents some original ideas, and may open a new investigation field because it also enables the evaluation of the iris behavior, e.g., the response time to the stimuli and the consequent alterations. That is, it can be used for investigations in ophthalmological areas (detection of optic nerve diseases) and public security (detection of alcohol levels), etc.

REFERENCES

[1] J. Daugman, "New methods in Iris recognition," *IEEE Trans. Syst., Man, Cybern. B, Cybern.*, vol. 37, no. 5, pp. 1167–1175, Oct. 2007.
[2] F. H. Adler, *Physiology of the Eye: Clinical Application*., 4th ed. London, U.K.: Mosby, 1965, p. 889.
[3] S. P. Narote, A. S. Narote, L. M. Waghmare, M. B. Kokare, and A. N. Gaikwad, "An iris recognition based on dual tree complex wavelet transform," in *Proc. TENCON—IEEE Region 10 Conf.*, Oct. 2007, pp. 1–4.
[4] J. Daugman, "How iris recognition works," in *Proc. Int. Conf. Image Process.*, Dec. 2002, vol. 1, pp. I-33–I-36.
[5] R. P. Wildes, "Automated iris recognition: An emerging biometric technology," *Proc. IEEE*, vol. 85, no. 9, pp. 1348–1363, Sep. 1997.
[6] W. W. Boles and B. Boashash, "A human identification technique using images of the iris and wavelet transform," *IEEE Trans. Signal Process.*, vol. 46, no. 4, pp. 1185–1188, Apr. 1998.
[7] P. J. Phillips, H. Moon, S. A. Rizvi, and P. J. Rauss, "The FERET evaluation methodology for face-recognition algorithms," *IEEE Trans. Pattern Anal. Mach. Intell.*, vol. 22, no. 10, pp. 1090–1104, Oct. 2000.
[8] R. Wildes, J. C. Asmuth, G. L. Green, S. C. Hsu, R. J. Kolczynski, J. R. Matey, and S. E. Mcbride, "A system for automated iris recognition," in *Proc. 2nd IEEE Workshop Appl. Comput. Vis.*, Dec. 05–07, 1994, pp. 121–128.
[9] X. Yuan and P. Shi, "Iris feature extraction using 2D phase congruency," in *Proc. 3rd ICITA*, Jul. 4–7, 2005, pp. 437–441.
[10] J. G. Ko, Y. H. Gil, and J. H. Yoo, "Iris recognition using cumulative sum based change analysis," in *Proc. ISPACS*, Japan, Dec. 12–15, 2006, pp. 275–278.

[11] L. Pan and M. Xie, "Research on iris image preprocessing algorithm," in *Proc. IEEE Int. Symp. Commun. Inform. Tech.*, Oct. 12–14, 2005, vol. 1, no. 14, pp. 161–164.
[12] Q. Tian, Z. Liu, L. Li, and Z. Sun, "A practical iris recognition algorithm," in *Proc. IEEE Int. Conf. Robot. Biomimetics*, Dec. 17–20, 2006, pp. 392–395.
[13] H. Meng and C. Xu, "Iris recognition algorithms based on gabor wavelet transforms," in *Proc. IEEE Int. Conf. Mechatron. Autom.*, Jun. 25–28, 2006, pp. 1785–1789.
[14] J. Wang and M. Xie, "Iris feature extraction based on wavelet packet analysis," in *Proc. Int. Conf. Commun., Circuits Syst.*, Jun. 2006, vol. 1, pp. 31–34.
[15] W. Tong and H. Pi-Lian, "A hidden markov model for iris recognition method," in *Proc. IEEE Int. Conf. Control Autom.*, Guangzhou, China, May 30–Jun. 1 2007, pp. 1791–1794.
[16] K. Hollingsworth, T. Peters, K. W. Bowyer, and P. J. Flynn, "Iris recognition using signal-level fusion of frames from video," *IEEE Trans. Inf. Forensics Security*, vol. 4, no. 4, pp. 837–848, Dec 2009.
[17] Y. Lee, P. J. Phillips, and R. J. Micheals, "An automated video-based system for iris recognition," in *Lecture Notes in Computer Science*, vol. 5558/2009. Berlin: Springer-Verlag, 2009, pp. 1160–1169.
[18] R. Zhu, J. Yang, and R. Wu, "Iris recognition based on local feature point matching," in *Proc. ISCIT*, Bangkok, Thailand, Oct. 2006, pp. 451–454.
[19] C. Liu and M. Xie, "Iris recognition based on DLDA," in *Proc. 18th Int. Conf. Pattern Recog.*, Hong Kong, 2006, vol. 4, pp. 489–492.
[20] M. Negin, T. A. Chmielewski, Jr., M. Salganicoff, U. M. von Seelen, P. L. Venetainer, and G. G. Zhang, "An iris biometric system for public and personal use," *IEEE Comput.*, vol. 33, no. 2, pp. 70–75, Feb. 2000.
[21] T. Kanade, A. Jain, and N. K. Ratha, "Audio- and video-based biometric person authentication," in *Proc. 5th AVBPA Int. Conf.*, vol. 3546, *Lecture Notes in Computer Science*, New York, Jul. 20–22, 2005, p. 1134.
[22] M. Walsh, *Nurse Practitioners: Clinical Skill and Professional Issues*., 2nd ed. London, U.K.: Butterworth-Heinemann, 2006, p. 388.
[23] J. D. Kibble and C. R. Halsey, *Medical Physiology: The Big Picture*., 1st ed. Beijing, China: McGraw-Hill, 2009, p. 448.
[24] K. D. Alloway and T. C. Pritchard, *Medical Neuroscience*., 2nd ed. Raleigh, NC: Hayes Barton Press, Dec. 25, 2007, p. 512.
[25] A. Longstaff, *Instant Notes in Neuroscience*., 2nd ed. Leeds, U.K.: Taylor & Francis, 2005, p. 468.
[26] R. S. Snell, *Clinical Neuroanatomy*., 7th ed. China: Lippincott Williams & Wilkins, 2010, p. 560.
[27] B. K. Sturges, "Neuro-ophthalmology: The visible nervous system," in *Proc. 2nd Annu. Veterinary Neurol. Symp.*, Davis, CA, 2005, p. 10.
[28] L. Ma, T. Tan, Y. Wang, and D. Zhang, "Personal identification based on iris texture analysis," *IEEE Trans. Pattern Anal. Mach. Intell.*, vol. 25, no. 12, pp. 1519–1533, Dec. 2003.
[29] R. M. Haralick and M. K. Shanmugam, "Computer classification of reservoir sandstones," *IEEE Trans. Geosci. Electron.*, vol. GE-11, no. 4, pp. 171–177, Oct. 1973.
[30] W. K. Pratt, *Digital Image Processing*., 4th ed. Hoboken, NJ: Wiley, 2007, p. 808.
[31] I. H. Witten, E. Frank, and M. A. Hall, *Data Mining Practical Machine Learning Tools and Techniques*., 3rd ed. Burlington, VT: Morgan Kaufmann, 2011, p. 664.

Ronaldo Martins da Costa was born at São Paulo's state, Brazil, in 1971. He received the B.S. and M.S. degrees in computer science from São Carlos Federal University, São Carlos, Brazil, in 1996 and 2002, respectively, and the Ph.D. degree from University of São Paulo, São Paulo, in 2010. His principal research interests include Programming Languages, Computer Vision, and Web Developments.

He is currently an Adjunct Professor at the Goiás Federal University, Brazil. From 1999 to 2004, he worked as Information Technology director at public services in Bauru, Brazil.

Adilson Gonzaga (M'11) was born at Minas Gerais, Brazil, in 1954. He received the B.S and M.S. degrees in electronic engineering and the Ph.D. degree in applied physics from the University of Sao Paulo, Sao Carlos, Brazil, in 1991.

He is an Associate Professor at University of Sao Paulo. Since 1973, he has been working at School of Engineering of São Carlos, Electrical Engineering Department, where he has done research in the field of Computer Vision, Image Processing and Biometry. He is the coordinator of the Computer Vision Laboratory (LAVI). His current research interest is Biometry, Robot Vision, Automated Visual Inspection, Pattern Recognition, Perception, and Artificial Intelligence.

Dr. Gonzaga is a member of Association for Computing Machinery and Brazilian Computer Society.